CHEMISTRY OF MATERIALS

ARTICLE

pubs.acs.org/cm

Aqueous Route to Biocompatible ZnSe:Mn/ZnO Core/Shell Quantum Dots Using 1-Thioglycerol As Stabilizer

Abdelhay Aboulaich,[†] Lavinia Balan,[‡] Jaafar Ghanbaja,[§] Ghouti Medjahdi,[#] Christophe Merlin,[⊥] and Raphaël Schneider*[,†]

[†]Laboratoire Réactions et Génie des Procédés (LRGP), UPR 3349, Nancy-University, CNRS, 1 rue Grandville, 54001 Nancy Cedex, France

[‡]Institut de Science des Matériaux de Mulhouse (IS2M), LRC 7228, 15 rue Jean Starcky, 68093 Mulhouse, France

[§]SCMEM and [#]IJL, Nancy-University, BP 70239, 54506 Vandoeuvre-lès-Nancy Cedex, France

[⊥]Laboratoire de Chimie Physique et Microbiologie pour l'Environnement (LCPME), UMR 7564 CNRS-Nancy-Université, 15 Avenue du Charmois, 54500 Vandoeuvre-lès-Nancy, France.

Supporting Information

ABSTRACT:

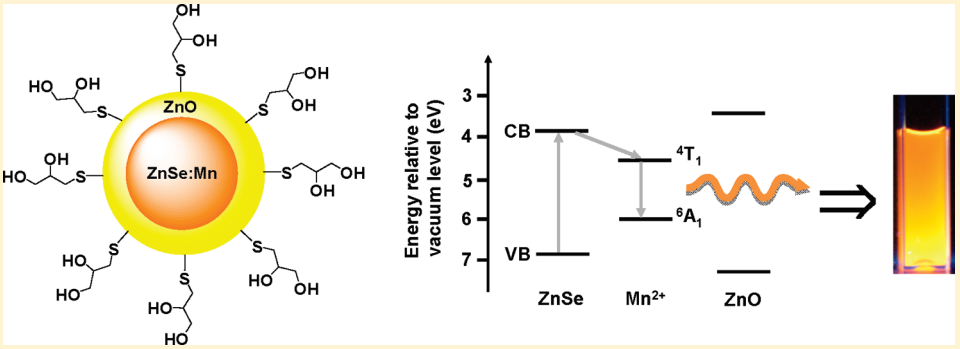

Water-dispersible 1-thioglycerol-capped Mn-doped ZnSe quantum dots (QDs) were prepared in aqueous solution through the nucleation-doping method by using safe and low-cost inorganic salts as precursors. Influence of the Zn/Se ratio, precursors concentrations and reaction pH on the particle size, colloidal stability, and photoluminescence (PL) were investigated. Under optimal conditions, thioglycerol-capped ZnSe:Mn QDs with an average diameter of 3.5 nm and a PL quantum yield of 3.5% in water at neutral pH were produced. X-ray powder diffraction, X-ray photoelectron spectroscopy, transmission electron microscopy, UV−visible spectroscopy and spectrofluorometry have been used to characterize the crystal structure and the optical properties of the dots. Remarkable improvements of stability in biological medium and PL were achieved by introduction of a ZnO shell through basic hydrolysis of $Zn(NO_3)_2$. ZnO was found to eliminate the surface-trap state from Mn^{2+}-doped ZnSe cores and enhance their PL quantum yield to 12%. Growth inhibition tests showed that core/shell ZnSe:Mn/ZnO@TG QDs do not exhibit any cytotoxicity toward *E. coli* bacterial cells up to a concentration of 0.14 mg/mL, indicating that these nanocrystals can be considered as building blocks for the synthesis of bioprobes for cells and tissues imaging.

KEYWORDS: quantum dots, Mn-doped ZnSe, thioglycerol, surface modification, ZnO, core/shell, photoluminescence, cytotoxicity

1. INTRODUCTION

Quantum dots (QDs) or semiconductor nanocrystals are of great interest to fundamental studies but have also potential applications as biological probes,[1,2] fluorescent biosensor,[3] light-emitting diodes (LEDs),[4] and solar cells.[5] Compared to conventional organic dyes, QDs possess many advantages, including high photoluminescence quantum yields (PL QYs), photobleaching stability, continuous absorption band, and size-tunable photoluminescence.[6−9] For biological labeling, the most studied QDs are the nanocrystals of CdSe and CdTe and the corresponding core/shell structured QDs (such as CdSe/ZnS, CdTe/ZnS, or CdTe/ZnTe) that are more robust against chemical degradation or photooxidation than the parent cores.[10,11] Unfortunately, the toxicity of cadmium is a concern that will limit the use of these visible or near IR emitting nanocrystals, especially for applications directly related to human health. With regard to the inherent problems of heavy metal-containing QDs, the search for alternative probes has become one of the most challenging aspect of working with these materials in biological

Received: May 6, 2011
Revised: July 12, 2011
Published: July 27, 2011

and medical fields. Promising Cd-free QDs are doped semiconductor nanocrystals.[12−15]

Doping with atomic impurities is an efficient way to manipulate the fluorescence emission spectra of wide bang gap semiconductors like ZnS or ZnSe that emit in the violet or blue region. A system of recent interest has been Mn^{2+}-doped ZnSe (ZnSe:Mn). In ZnSe:Mn dots, a small amount of Mn^{2+} is incorporated into the host ZnSe nanocrystalline lattice, which results in visible fluorescence at ca. 590 nm attributed to a $^4T_1 \rightarrow {}^6A_1$ transition of Mn^{2+} ions in T_d symmetry.[16,17] Moreover, doping with Mn^{2+} can impart remarkable magneto-optical properties to QDs.[18]

In the past decade, numerous organometallic routes were reported to synthesize ZnSe:Mn QDs.[19−26] These syntheses require pyrolysis (around 300 °C) in hot coordinating solvents such as tri-n-octylphosphine (TOP), tri-n-octylphosphine oxide (TOPO) and hexadecylamine (HAD), followed by the crystal growth at lower temperature (typically between 200 and 300 °C). QDs thus produced are capped by hydrophobic ligands and are only dispersible in low polar organic solvents such as toluene or chloroform.

Direct synthesis of ZnSe:Mn QDs in water is a promising alternative route to organometallic reactions and facilitates the use of the dots in biological systems. Hydrothermal synthesis offers also the following advantages: (1) lower reaction temperature (80−100 °C) with comparable PL QY; (2) does not use toxic and expensive organometallic reagents; (3) surface functionalization during synthesis without further treatment; (4) comparatively smaller sizes (3−8 nm) than those obtained after encapsulation of hydrophobic QDs with amphiphilic lipids or polymers (generally >20 nm); (5) more reproducible. Significant advances have been made in the aqueous synthesis of ZnSe:Mn QDs during the past two years. Wang et al. have reported the first aqueous route to ZnSe:Mn QDs capped by 3-mercaptopropionic acid (MPA).[27] This method was very recently extended to color-tunable ZnSe:Mn QDs.[28] Fang et al.[29] and our group[30] have very recently described the preparation of core/shell ZnSe:Mn/ZnS@MPA QDs in aqueous media with improved PL QYs compared to the ZnSe:Mn cores.

The interface between the organic molecules stabilizing the QD dispersion and the surrounding medium largely influences the colloidal properties of the nanoparticles, such as the hydrodynamic size, charge and intermolecular/interparticle interactions. Hydrophilic thiols bind to QD surface atoms and simultaneously stabilize QD dispersions in polar solvents, and as such, are responsible for the surface-related optical properties of the QDs. 1-Thioglycerol (TG) is an effective size-regulating and stabilizing agent for II−VI semiconductor nanocrystals.[31−37] On the basis of the classical model of La Mer, the nucleation is followed by crystal growth via coalescence and fusion of smaller clusters.[38,39] Because the two hydroxyl groups of TG are partially charged at pH values higher than 9, TG was found to significantly affect coalescence and fusion of ionic monomers or clusters during CdSe and CdTe QDs syntheses.

Herein, for the first time, we describe the preparation of TG-capped ZnSe:Mn QDs in aqueous solution using a mixture of the dopant and of the host precursor during the nucleation step (also called nucleation-doping strategy). The resulting QDs grown by this alternative method were found to be with high optical quality. Only pure dopant emission at ca. 590 nm without trap state emission was observed. Capping QDs with inorganic shells is an efficient strategy to optimize their PL QYs, surface functionality, and photochemical stability. A few studies, however, have demonstrated that introduction of an inorganic shell at the surface of TG-capped QDs is often problematic[36,40] and could only efficiently be achieved by ultrasonic irradiation of aqueous dispersions of the nanocrystals in the thiourea used to deposit a sulfur containing shell.[41] In this work, we take advantage of the hydroxyl groups of TG to use TG-capped ZnSe:Mn QDs as template cores to introduce a ZnO shell. This passivation allows a marked improvement of the emission properties of the nanocrystals. The core/shell ZnSe:Mn/ZnO@TG QDs have a PL QY of 12% in water at neutral pH.

2. EXPERIMENTAL SECTION

2.1. Reagents and Materials. Zinc sulfate heptahydrate ($ZnSO_4 \cdot 7H_2O$, 99.99%), zinc nitrate hexahydrate ($Zn(NO_3)_2 \cdot 6H_2O$, 98+%), manganese acetate tetrahydrate ($Mn(OAc)_2 \cdot 4H_2O$, 99%), 1-thioglycerol (TG, 99%), selenium powder (99.5%, 100 mesh), sodium borohydride ($NaBH_4$, 98%), and acetone (HPLC grade) were used as received without additional purification. All solutions were prepared using Milli-Q water (18.2 MΩ cm^{-1}, Millipore) as the solvent.

2.2. Synthesis of TG-Capped ZnSe:Mn QDs. The preparation of NaHSe was performed according to Klayman et al.[42] with some modifications. Under an argon atmosphere, 76 mg (2.009 mmol) of $NaBH_4$ was added to a small flask cooled with ice containing 1 mL of ultrapure water. 79 mg (1.004 mmol) of selenium powder was then added and a small outlet was connected to the flask to discharge the hydrogen pressure generated by the reduction of Se into NaHSe. After 3 h at 4 °C, the black selenium powder disappeared and a white NaHSe solution was obtained. The solution was diluted with 19 mL of argon-saturated water and the concentration of the final NaHSe solution was 0.05 M.

In a typical procedure, solutions of 0.1 M $ZnSO_4 \cdot 7H_2O$ (5 mL), 0.01 M $Mn(OAc)_2 \cdot 4H_2O$ (2 mL) for a Mn^{2+} doping of 4% relative to Zn^{2+} and 0.1 M TG (20 mL) were mixed and the pH of the mixture was adjusted to 9.5 by dropwise addition of a 2 M NaOH solution. The molar ratio Zn^{2+}/Se^{2-}/TG in the solution was 1/0.9/4. The solution was placed in a three-necked flask fitted with a septum and valves, and further stirred under argon for 1 h. Nine mL of a freshly prepared NaHSe solution (0.05 M) were then injected through a syringe into the mixture at room temperature. Subsequently, the reaction mixture was heated to reflux at 100 °C for 16 h under argon flow with a condenser attached. The reaction was terminated by allowing the reaction mixture to cool down to room temperature. The obtained TG-capped ZnSe:Mn nanocrystals were purified by centrifugation in acetone, washed 3 times with acetone, and then dried in vacuum at room temperature for 2 h before measurements.

2.3. Deposition of ZnO Shell around ZnSe:Mn QDs. For the ZnO shell growth, a simple procedure based on hydrolysis and condensation of $Zn(NO_3)_2$ in basic medium was adopted. Typically, 20 mg of ZnSe:Mn QDs were dispersed in 40 mL of water. The pH was adjusted to 10 with 0.1 M NaOH. Then, an appropriate amount of 0.05 M $Zn(NO_3)_2.6H_2O$ aqueous solution was added dropwise to the ZnSe:Mn@TG suspension under vigorous stirring at room temperature. The ZnO/ZnSe:Mn molar ratio was varied (by varying the volume of 0.05 M $Zn(NO_3)_2.6H_2O$ aqueous solution) from 0.05 to 0.3. The reaction mixture was concentrated down to approximately 5 mL, TG-capped core/shell ZnSe:Mn/ZnO nanocrystals were precipitated with acetone and dried in vacuum (30 mmHg, 2 h, room temperature).

2.4. Instrument. Transmission electron microscopy (TEM) images were taken by placing a drop of the particles in water onto a carbon film-supported copper grid. Samples were studied using a Philips CM20 instrument operating at 200 kV equipped with Energy-dispersive X-ray Spectrometer (EDS). The X-ray powder diffraction (XRD)

dx.doi.org/10.1021/cm2012928 |Chem. Mater. 2011, 23, 3706–3713

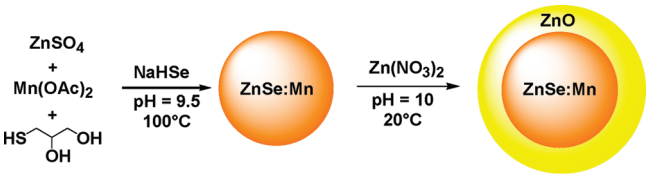

Figure 1. Schematic representation of the two-step synthesis of ZnSe:Mn/ZnO@TG core/shell QDs.

diagrams of all samples were measured using Panalytical X′Pert Pro MPD diffractometer using Cu Kα radiation. The average particle size was calculated from line broadening using the Topas application (Bruker XAS). We used the Fundamental Parameters approach (FP)[43] and the instrumental broadening was determined using standard LaB6 powder. The X-ray powder diffraction data were collected from an X′Pert MPD diffractometer (Panalytical AXS) with a goniometer radius 240 mm, fixed divergence slit module (1/2° divergence slit, 0.04 rd Sollers slits) and an X′Celerator as a detector. The powder samples were placed on zerobackground quartz sample holders and the XRD patterns were recorded at room temperature using Cu K_α radiation (λ = 0.15418 nm).

XPS measurements were performed at a residual pressure of 10^{-9} mbar, using a KRATOS Axis Ultra electron energy analyzer operating with an Al Kα monochromatic source. Absorption spectra were recorded on a Perkin-Elmer (Lambda 2) UV−visible spectrophotometer. Fluorescence spectra were recorded on a fluorolog-3 spectrofluorimeter *F*222 (Jobin Yvon) using a 450 W xenon lamp. The QY values were determined from the following equation:

$$QY(sample) = (F_{sample}/F_{ref})(A_{ref}/A_{sample})(n_{samlpe}{}^2/n_{ref}{}^2)QY_{(ref)}$$

where *F*, *A*, and *n* are the measured fluorescence (area under the emission peak), absorbance at the excitation wavelength and refractive index of the solvent respectively. PL spectra were spectrally corrected and quantum yields were determined relative to Rhodamine 6G (QY = 94%).[44] The fluorescence lifetimes were measured by a FluoroMax-4 spectrofluorometer (Jobin Yvon) using a NanoLED emitting at 372 nm as an excitation source with a nanoled controller module, Fluorohub from IBH, operating at 1 MHz. The detection was based on an R928P type photomultiplier from Hamamatsu. Fourier transform infrared spectroscopy (FT-IR) was performed using a Bruker Vector 22 spectrometer. Dynamic light scattering (DLS) was performed at room temperature using a Malvern zetasizer HsA instrument with a He−Ne laser (4×10^{-3} W) at a wavelength of 633 nm. The QDs aqueous solutions were filtered through Millipore membranes (0.2 μm pore size). The data were analyzed by the CONTIN method to obtain the hydrodynamic diameter (d_H) and the size distribution in each aqueous dispersion of nanoparticles.

2.5. Cytotoxicity Tests. Bacteria were routinely cultured at 30 °C in 100 mL conical flasks filled with 20 mL of MOPS-buffered RM medium[45] supplemented with 0.2% gluconate, 0.02 mM Fe(+3)-(NH_4)citrate and 0.1% (v/v) of the trace elements solution SL 7 of Biebl and Pfennig,[46] using an Innova 3100 water bath shaker (New Brunswick) set at 160 rpm. Growth inhibition tests were carried out on *Escherichia coli* MG1655[47] as previously described.[48] Briefly, bacteria were pregrown in RM medium without QDs until the cultures reached midlog phase (optical density [OD] at 600 nm around 0.2). Cultures were then diluted one-tenth in prewarmed amended RM medium supplemented with the desired concentration of QDs and the DO_{600} was measured at intervals of 20 min (using a UVmc2 safas spectrometer UV−visible spectrometer). The doubling times of exponentially growing cultures were calculated and compared from one experiment to another in order to evaluate the toxic effect of a given QD when compared to the control (extended doubling time). Typically, under these conditions, *E. coli* MG1655 exhibits a doubling time of 119 min with a standard deviation of 8 min in absence of QDs.

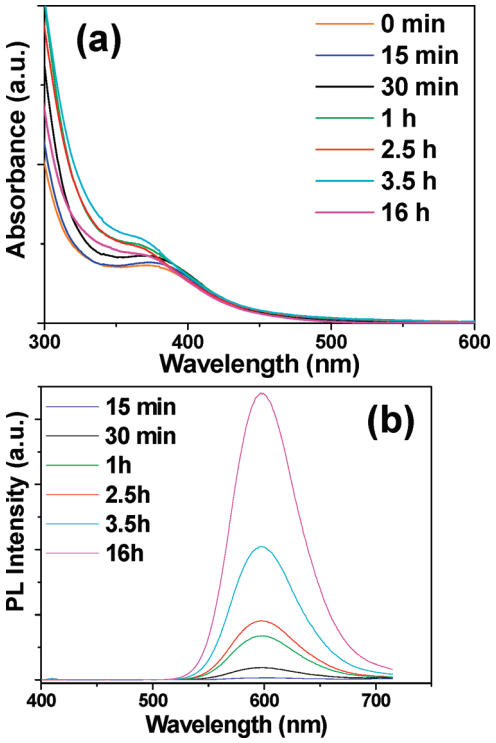

Figure 2. Temporal evolution of (a) UV−visible and (b) photoluminescence spectra of ZnSe:Mn@TG QDs during the growth of nanocrystals at 100 °C.

3. RESULTS AND DISCUSSION

A two-step procedure was adopted for the preparation of core/shell ZnSe:Mn/ZnO QDs. In the first step, thioglycerol-capped ZnSe:Mn core QDs were prepared using a mixture of the dopant and of the host precursor. The ZnSe:Mn cores were further overcoated with different thicknesses of ZnO shell in aqueous solution through precipitation reaction (Figure 1).

3.1. Influence of Precursors Ratio, pH, and Concentrations on ZnSe:Mn Core Synthesis. The aqueous synthesis of ZnSe:Mn core nanocrystals commences with the reaction between Zn^{2+}, Mn^{2+}, and Se^{2-} in the presence of TG at room temperature. Similarly to our previous report,[30] we found that good quality ZnSe:Mn@TG QDs (PL QY = 3.5%) were obtained (i) using NaHSe in short supply (by ca. 0.9-fold) relative to the mole amount of the Zn^{2+} precursor, and (ii) using 4% Mn^{2+} relative to Zn^{2+}. All samples prepared with Se/Zn ratios higher than 1 showed almost no Mn^{2+} emission but only ZnSe bandgap emission together with strong trap emission. The pH of the reaction mixture played a determining role for the reproducibility of the synthesis. If the preparation of TG-capped ZnSe:Mn QDs is conducted at pH 10.3 like described for MPA-capped ZnSe:Mn QDs, a brown color, most likely associated to the high susceptibility of the primary formed Mn^{2+}/thioglycerol clusters to yield manganese oxide or hydroxide at pH > 10, appeared in the reaction flask. The formation of these compounds was avoided by performing the reaction at pH 9.5.

We also explored the aqueous growth at different precursor concentrations ranging from 1 to 10 mM, whereas other experimental

dx.doi.org/10.1021/cm2012928 |*Chem. Mater.* 2011, 23, 3706–3713

conditions were kept the same: the molar ratio of $Zn^{2+}/Mn^{2+}/TG/HSe^-$ was 1/0.04/4/0.9, pH 9.5, and temperature =100 °C. A fast crystal growth was observed at the early stage of the reaction and was accelerated by lowering the precursor concentration in the reaction medium. Moreover, ZnSe:Mn@TG QDs synthesized at low precursor concentration have a better quality as compared to those produced at higher concentration and exhibit only pure dopant emission (>99% in intensity). It was finally observed that the QDs derived from the more concentrated solutions of precursors (>3 mM) led to formation of macroscopic aggregates either during the heating period or upon storage at room temperature of the crude colloidal solutions.

ZnSe:Mn QDs obtained at low precursor concentration (2.7 mM or less) usually exhibit a prominent absorption band, leading to a distinguished temporal evolution of the QD size. A typical temporal evolution of the ZnSe:Mn@TG grown at 100 °C with a Zn^{2+} concentration of 2.7 mM is shown in Figure 2a. Immediately after the injection of NaHSe (t = 0 min), an absorption band centered at 370 nm was observed indicating the rapid formation of the ZnSe host material. The growth of the nanocrystals during reflux is indicated by a low-energy shift from 370 to 378 nm after 30 min heating. Figure 2a shows also that the absorption band of ZnSe:Mn QDs becomes broader and more dissymmetric after 1 h heating, suggesting a broadening of QDs size distribution due to Ostwald ripening (small nanocrystals dissolve in the reaction medium while larger ones keep growing). The progressive blue-shift observed after 1 h reflux (368 nm after 16 h heating) may be due to the release of S^{2-} by the partial decomposition of TG at 100 °C, leading to a sulfur-enriched shell.

The corresponding PL spectra are given in Figure 2b. The initial PL is negligible and only a very weak trap-emission band at ca. 480 nm was observed. The pseudotetrahedral ($^4T_1 \rightarrow {}^6A_1$) transitions of the Mn^{2+} ions incorporated into the ZnSe dots could already be observed after 15 min reflux, increased gradually and reached its maximum value after 16 h heating. The PL QY measured from the purified ZnSe:Mn@TG QDs prepared under these synthetic conditions and dispersed in water at neutral pH is 3.5%. Because Mn^{2+} has a lower reactivity than Zn^{2+} toward Se^{2-},[49] we suppose that Mn^{2+} ions are not incorporated into the ZnSe lattice at the early stage of growth. Indeed, Mn^{2+} ions have to be incorporated into the host lattice and be isolated from the solution environment before they can act as electron−hole recombination centers that give rise to dopant photoluminescence.[21] In the current work conducted with TG as ligand, we also found that the room-temperature PL emission spectra obtained after excitation at 360 nm exhibit the Mn^{2+}-related $^4T_1 \rightarrow {}^6A_1$ photoluminescence at 598 nm regardless of the heating time. As recently observed by us and others,[20,30] during aqueous syntheses of ZnSe:Mn QDs capped by MPA, the d-orbitals of the Mn^{2+} centers of doped ZnSe QDs will experience a high electric field difference along different directions because of the negatively charged MPA ligand, which results in a higher splitting of the energy levels. The crystal field for each Mn^{2+} ion is more symmetric for syntheses conducted with TG, and consequently, the crystal field splitting of the d-orbitals is less affected by the ligand surrounding the nanocrystals. These results demonstrate also a clear decoupling of the nucleation-doping and of the growth steps and indicate that the host ZnSe semiconductor layer grew epitaxially onto the surface of the doped ZnSe:Mn particles.

3.2. Size, Shape, Crystal Structure, and PL Properties of TG-Capped ZnSe:Mn Dots. Figure 3a shows wide-field TEM image together with a representative high-resolution TEM

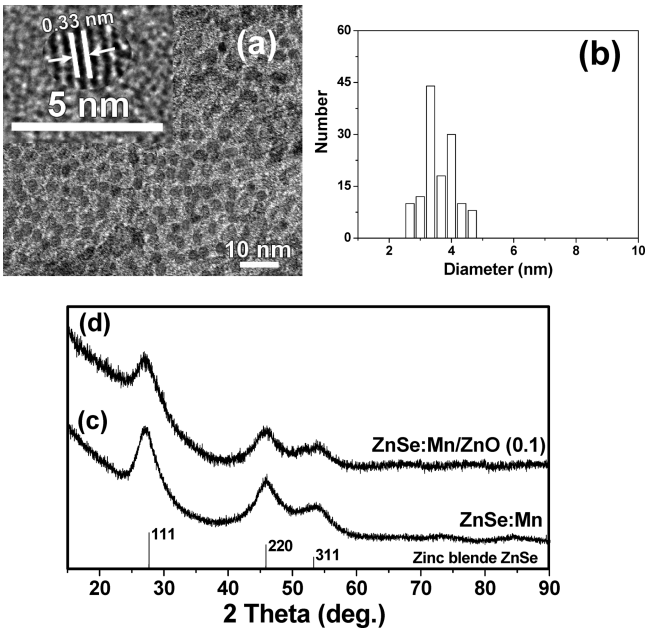

Figure 3. (a) TEM image of ZnSe:Mn@TG QDs. A representative HRTEM is given as the inset. (b) Corresponding particle size distribution. XRD patterns of ZnSe:Mn@TG QDs (c) before and (d) after introduction of the ZnO shell.

(HRTEM) image of ZnSe:Mn@TG QDs obtained after 16 h heating at 100 °C. The dots are seen to be uniform, disperse and have an average size of 3.6 ± 0.5 nm, which is slightly larger than ZnSe:Mn QDs capped by MPA prepared under similar conditions.[30] The HRTEM image indicates the distances between the adjacent lattice fringes to be 0.32 nm, value consistent with the literature value for the (111) d spacing, 0.324 nm (JCPDS 80−0021), which shows the ZnSe:Mn@TG dots are in the cubic phase.

The powder XRD patterns recorded from ZnSe:Mn@TG solid sample precipitated from aqueous solution with an excess of acetone are shown in Figure 3c. No diffraction peaks from impurities were detected in the sample. The intense and wide peaks, characteristic for nanoparticles, are positioned at 2θ = 26.9, 45.8, and 53.2°, which oriented along the (111), (220), and (311) directions, and are in agreement with the JCPDS file 80−0021 for cubic zinc blende ZnSe. This result shows that Mn^{2+} doping into the ZnSe host nanocrystals does not disturb the crystal structure. Using the Rietveld refinements with the Fundamental Parameters approach built-in Topas application, a crystallite size of 2.7 ± 0.3 nm with a standard deviation (anisotropy) of 0.2 nm was calculated. It is also worth noting that the diffractive peaks for ZnSe:Mn@TG QDs are located at higher angle compared to that of pure ZnSe probably because the TG ligand partially decomposed during the heating phase leading to nanocrystals with a ZnS-rich surface (also called gradient core/shell nanocrystals).

Since XPS is powerful for identifying the compositions and structures of the surface of nanosized materials, it was used to characterize the ZnSe:Mn@TG nanocrystals (see Figure S1 in the Supporting Information). The binding energies of 1019.5 and 53.9 eV correspond respectively to the Zn 2p and Se 3d levels. Because XPS is mostly sensitive to the surface atoms, it is not surprising that Mn could not be observed in the ZnSe:Mn QDs obtained after 16 h heating at 100 °C. This result also

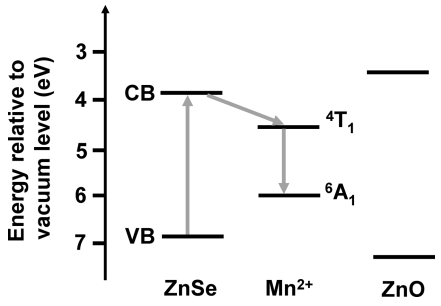

Figure 4. Schematic energy level diagram for ZnSe:Mn/ZnO core/shell nanocrystals. The transition from $Mn^{2+4}T_1$ state to the $^6A_1$ state results in orange light emission.

corroborates our hypothesis that Mn^{2+} ions are close to the center of the dots and surrounded by a relatively uniform environment as previously observed in PL emission spectra.

Mn^{2+} ions could however be detected through Energy Dispersive Spectroscopy (EDS) measurements conducted on purified QDs (see Figure S2 in the Supporting Information). The Mn^{2+} at % was found to be 3.2%, value close to the theoretical dopant concentration in the dots (4%). This result indicates also that Mn^{2+} ions are substitutionally incorporated into the ZnSe host lattice. Finally, the atomic composition of the QDs is close to that of the ratios of precursors (experimental Zn/Se ratio of 1.18). An average diameter of 3.6 nm represents about 139 ZnSe structural units in each nanocrystal (using a theoretical lattice parameter a of 0.56 nm, JCPDS file No 80−0021). Using 3.2% Mn^{2+} dopant means about 18 Mn^{2+} ions per nanocrystal.

The capping of ZnSe:Mn QDs by 1-thioglycerol was also confirmed by FTIR spectroscopy (see Figure S3 in the Supporting Information). The FTIR spectrum of the nanocrystals is similar to that of 1-thioglycerol except for the absence of the S−H vibration band at 2557 cm^{-1} because the thiolate functions of the TG ligands are connected to the Zn^{2+} sites on the ZnSe nanocrystals surfaces.

Absorption, PL and PL excitation (PLE) spectra for the ZnSe:Mn@TG QDs obtained after 16 h heating are shown in Figure S4 in the Supporting Information. A strong orange emission around 596 nm is evident in the PL spectrum of ZnSe:Mn dots, and the PLE spectrum shows the optimal excitation wavelength for the orange emission is 377 nm. Using Rhodamine 6G as reference, a PL QY of 3.5% was evaluated.

Equation 1 shows the relationship between the radius r of spherical nanocrystals and their band gap E, using the formula of Brus based on the effective mass approximation.

$$E = E_g + \frac{\hbar^2\pi^2}{2r^2}\left(\frac{1}{m_e} + \frac{1}{m_h}\right) - \frac{1.8e^2}{\varepsilon r} \quad (1)$$

where E_g is the band gap of the bulk material (2.80 eV, 460 nm), $\hbar$ is the reduced Plank's constant (6.58×10^{-16} eV), e is the charge of the electron (1.6×10^{-19} C), ε is the semiconductor dielectric constant (9.2), m_e and m_h are effective masses of the electrons and holes, respectively, and m_o is the free electron mass ($m_o = 9.11 \times 10^{-28}$ g). With the effective masses of electrons ($m_e = 0.15\ m_o$) and holes ($m_h = 0.66\ m_o$) and using the absorption peak for TG-capped ZnSe:Mn QDs after 16 h growth yields a nanocrystal diameter of 3.42 ± 0.4 nm, which is in good agreement with the diameters obtained from the TEM data. The deviation of 0.4 nm corresponds to ±10 nm for the determination of the onset of absorption.

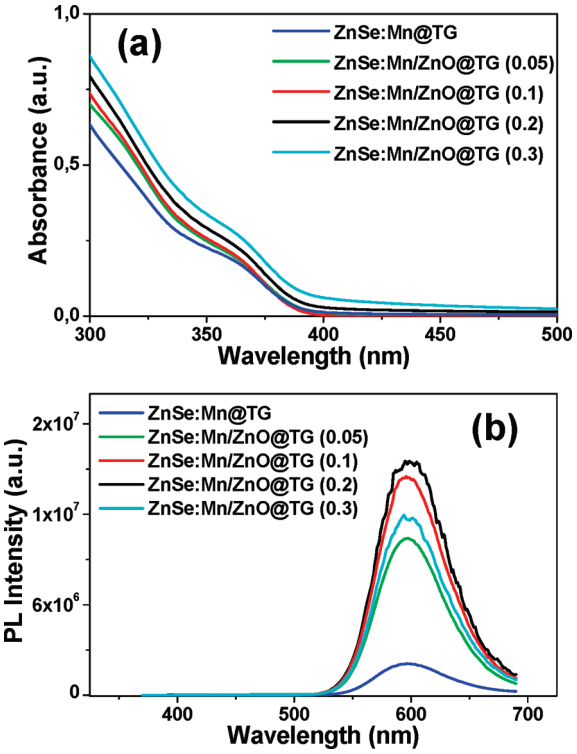

Figure 5. Evolution of absorption and PL emission of ZnSe:Mn QDs upon addition of the ZnO shell. Excitation wavelength is 360 nm.

3.3. Epitaxial Growth of the ZnO Shell. In general, the maximum PL QY is directly related to a minimum density of surface-trap states on nanocrystals.[50−52] An important strategy to improve QDs' surface passivation is their overgrowth with a shell possessing a wider band gap than that of the core (type I core/shell nanocrystals).[53] Consequently, both electrons and holes are confined in the core and radiative recombinations are improved (Figure 4).

Attemps to add a ZnS shell according to our previous report[30] were unsuccessful with ZnSe:Mn@TG QDs. Only large precipitates accompanied by the loss of fluorescence were observed during the decomposition of Zn^{2+}/MPA complexes at 100 °C in the presence of ZnSe:Mn@TG QDs. Introduction of a shell on the core nanocrystals requires generally a lattice matching between shell and core materials to achieve a better passivation and minimize the structure defects.[54] Despite the high lattice mismatch between ZnSe and ZnO (37%), we were pleased to find out that a thin ZnO shell could successfully be installed at the surface of ZnSe:Mn@TG QDs. Among the various Zn^{2+} salts tested for the ZnO capping ($Zn(OAc)_2$, $ZnSO_4$, $Zn(NO_3)_2$), best results were obtained with $Zn(NO_3)_2$. In alkaline conditions, $Zn(NO_3)_2$ is hydrolyzed into $Zn(OH)_2$, which dehydrates to produce ZnO clusters that grow at the surface of ZnSe:Mn nanocrystals to form the ZnO shell (Figure 1). Using a $Zn(NO_3)_2$/ZnSe:Mn molar ratio of 0.1, a marked decrease of pH from 10 to 8 was observed during the addition of $Zn(NO_3)_2$, thus confirming the consumption of NaOH in the hydrolysis reaction. As can be observed in Figure 5, the PL emission intensity increases markedly for $Zn(NO_3)_2$/ZnSe:Mn molar ratio of 0.05 (PL QY of 9%), reached its maximum value for a ratio of

dx.doi.org/10.1021/cm2012928 |Chem. Mater. 2011, 23, 3706–3713

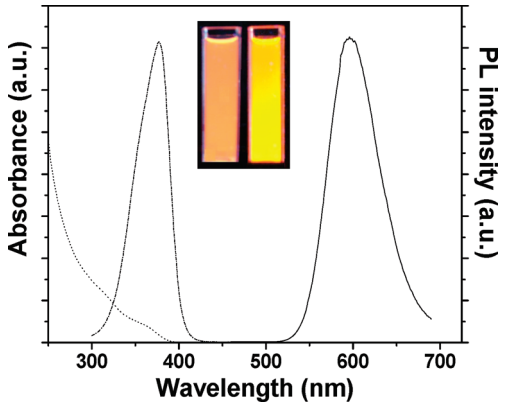

Figure 6. Optical absorption (dotted line), PL excitation (dashed line), and PL emission (solid line) after excitation at 360 nm of core/shell nanocrystals prepared with a ZnO/ZnSe:Mn ratio of 0.1. Inset shows digital pictures of the QDs before (left) and after (right) the overcoating with ZnO.

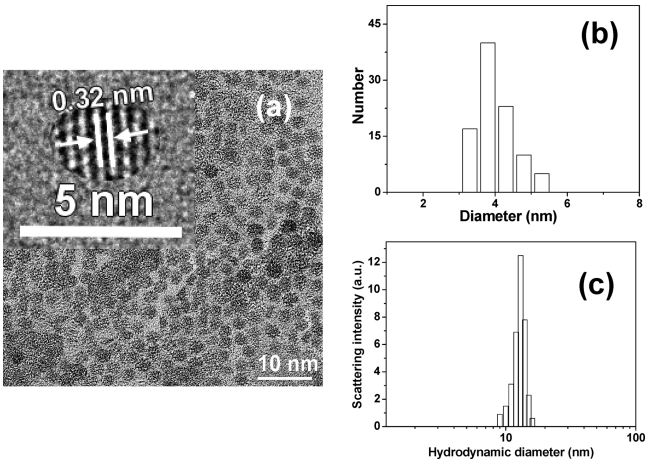

Figure 7. (a) TEM and HRTEM (inset) images of ZnSe:Mn/ZnO core/shell nanocrystals, (b) the corresponding particle size distribution, and (c) hydrodynamic size of ZnSe:Mn/ZnO dots measured by DLS.

0.1 (PL QY = 12%) and then decreased as the shell thickness growth (7.2 and 5.8% PL QYs for $Zn(NO_3)_2$/ZnSe:Mn ratios of 0.2 and 0.3, respectively). Similar observations made on core/shell/shell CdTe/CdS/ZnO QDs were ascribed to a saturation effect.[9] The PL QY of ZnSe:Mn/ZnO core/shell QDs (ZnO/ZnSe:Mn ratio of 0.1) is 12%, which compares favorably when compared to the QY of ZnSe:Mn QDs capped by 3-mercaptopropionic acid.[27−30] The final ZnSe:Mn/ZnO materials were also found to be stable in ambient conditions for months.

A visual comparison of uncoated and of the ZnO-coated QDs prepared using a molar ratio ZnO/ZnSe:Mn of 0.1 is shown as inset in Figure 6. Both samples are fluorescent under a hand-held UV lamp providing 366 nm multiband irradiation, and it is obvious that the ZnO-passivated d-dots are much brighter. Spectroscopic measurements show that the distinctive absorption and emission profiles of QDs after ZnO coating are preserved. No change in peak position of emission and excitation was observed for core/shell nanocrystals prepared with a ZnO/ZnSe:Mn ratio of 0.1 probably because the thickness of the ZnO shell around the ZnSe:Mn core is too weak to induce a significant effect on the photophysical properties of the nanocrystals. A quite similar result was observed by Jiang et al. when overcoating uncapped ZnS:Mn nanocrystals with a ZnO shell.[55]

Using TEM, the average diameter of ZnSe:Mn/ZnO core/shell nanocrystals prepared with a ZnO/ZnSe:Mn ratio of 0.1 was found to be 4.0 ± 0.5 nm (Figure 7). From the HRTEM image, the lattice spacing (0.32 nm) agrees well with that of the ZnSe:Mn core indicating that the introduction of the ZnO shell keeps unchanged the lattice spacing of ZnSe nanocrystals. Because the ZnO layer introduced at the periphery of ZnSe:Mn@TG QDs is very thin, it is difficult to recognize the interface by image contrast, even if the core and the shell do not have the same crystal structure. These results are consistent with the XRD pattern of ZnSe:Mn/ZnO core/shell nanocrystals (Figure 3d) which exhibited no shift from the original positions of ZnSe:Mn core nanocrystals. Calculation of the crystallite size resulted in 3.4 ± 0.8 nm, which correlates well with the value obtained from TEM analysis (4.0 nm). Apparently, the introduction of the ZnO shell around the ZnSe:Mn core does not cause aggregation, which is also confirmed by dynamic light scattering (DLS) measurements in aqueous solution. The DLS results showed a hydrodynamic diameter of 13.2 ± 2.4 nm, much larger than the particle size. This can be explained by the thiol ligands outspread in aqueous solution while they are highly contractive after drying on TEM copper grids but also by the solvatation layer around the QDs in aqueous media.

The slow PL decay curves of Mn^{2+} ions for the core ZnSe:Mn@TG and the core/shell ZnSe:Mn/ZnO@TG QDs are shown in Figure S5 in the Supporting Information. The slow decay times, attributed to the emission of the single isolated Mn^{2+} ions in a cubic site,[56−58] were 0.66 and 0.82 ms for the core and core/shell QDs, respectively. The enhancement observed for ZnSe:Mn/ZnO QDs is a direct consequence of the deeper embedding of Mn^{2+} emission centers in the nanocrystals and of their increased isolation from the surface defects.

3.4. Effect of pH and Saline Levels on TG-Capped ZnSe:Mn and ZnSe:Mn/ZnO QDs PL. For biological applications, QDs should be stable between pH 5 and 8, because (*i*) most bioconjugation reactions are performed in this pH range and because (*ii*) pH values found in the human body also fall in this range. QDs are however sensitive to chemicals in their surrounding environment such as acids, bases, metallic ions and biomolecules like proteins. For example, pH values can be directly correlated with QDs' PL intensity because QD fluorescence is, in general, enhanced in basic medium and quenched in acidic one.[59] Contrary to MPA-capped ZnSe:Mn core QDs which exhibit the highest PL QY at pH 12, TG-capped ZnSe:Mn QDs show the highest PL for pH values ranging from 8 to 10 (PL QY = 5.3% for ZnSe:Mn@TG QDs and 12.0 for ZnSe:Mn/ZnO@TG QDs at pH 9) (see Figure S6 in the Supporting Information). Rapid decays of PL intensity are observed for pH values below 6 or above 11. Under pH 4, the QDs became unstable in the aqueous environment, they precipitated and the PL disappeared.

The stability of the ZnSe:Mn/ZnO QDs in highly electrolytic environments is also an important issue for potential biological applications as well as for long-term storage. To evaluate this stability in different media, we dispersed ZnSe:Mn/ZnO QDs into deionized water (DI) (as a control) and 3-(*N*-morpholino)propanesulfonic acid (MOPS)-medium. Due to the sensitivity of the QDs photoluminescence to processes occurring at the nanocrystals surface, UV−vis absorbance and fluorescence peak position and intensity were used to monitor their stability. In DI,

dx.doi.org/10.1021/cm2012928 |*Chem. Mater.* 2011, 23, 3706–3713

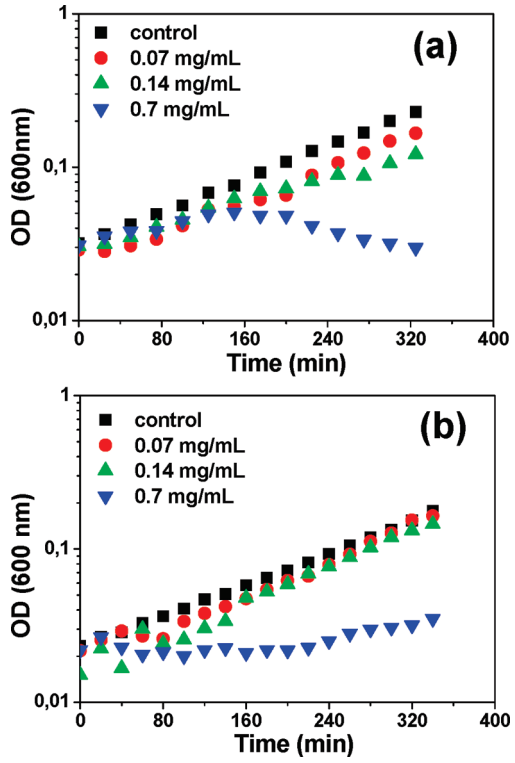

Figure 8. Growth inhibition of *E. coli* MG 1655 by (a) ZnSe:Mn@TG and (b) ZnSe:Mn/ZnO@TG QDs. MG 1655 was cultivated in RM medium until OD_{600} reached 0.2 and was diluted in RM medium supplemented with various concentrations of ZnSe:Mn core QDs.

the photophysical properties of the dots remained unchanged for at least 2 weeks. Similar behavior was observed in MOPS, which contains 80 mmol/L of NaCl. We saw the stability results obtained in the MOPS medium as an initial screening test for compatibility with physiological conditions.

3.5. Cytotoxicity. Because in vivo bioimaging and drug delivery are expected to be some of the major applications for QDs, we finally evaluated the cytotoxicity of core ZnSe:Mn and core/shell ZnSe:Mn/ZnO QDs using a simple and sensitive test based on growth inhibition of *E. coli* cells (Figure 8).[48] At 0.07 mg/mL, neither of the two QDs exhibited any cytotoxic effect as evidenced by generation times matching those of control cultures (119 ± 8 min). It is worth mentioning that this concentration is far higher than those classically used for in vitro or in vivo imaging with QDs (μM to nM concentrations). For ZnSe:Mn@TG QDs, the first signs of cytotoxicity appeared as altered growth rates past 160 min of cultivation, for concentrations of 0.14 and 0.7 mg/mL, where an extended generation time (ca. 204 min.) and cell lysis could be observed, respectively. On the contrary, the core/shell ZnSe:Mn/ZnO@TG nanocrystals displayed no toxicity until a concentration of 0.7 mg/mL where a growth arrest could be seen early after QD addition. This tends to demonstrate that the ZnO protective shell not only enhances the brightness of the dots but also improves their compatibility with biological material.

4. CONCLUSION

We have demonstrated a simple effective method for producing photoluminescent and water-dispersible thioglycerol-capped Mn-doped ZnSe nanocrystals and core/shell ZnSe:Mn/ZnO QDs. The structure, optical properties, and cytotoxicity have been studied. The fabricated ZnSe:Mn QDs overcoated by a thin ZnO shell have small diameters (ca. 4 nm) and hydrodynamic diameters (ca. 13 nm) and possess a good photoluminescence quantum yield (12%). Surprisingly and despite the high lattice mismatch between the core ZnSe material and the ZnO shell, this combination yields nanocrystals with lower cellular toxicity and better biocompatibility and photostability than the parent core QDs. We also note that the current work is mainly focused on technology development and characterization of the new nanocrystals prepared. Applications of these nanoprobes in bioimaging and nanodiagnostic are currently under investigation.

■ ASSOCIATED CONTENT

Supporting Information. XPS, EDX, and FT-IR spectra, optical absorption, PL excitation and PL emission spectra of ZnSe:Mn@TG QDs, PL decay curves of ZnSe:Mn and ZnSe:Mn/ZnO QDs, and effect of the pH on the PL quantum yield of ZnSe:Mn@TG and ZnSe:Mn/ZnO@TG QDs. This material is available free of charge via the Internet at http://pubs.acs.org.

■ AUTHOR INFORMATION

Corresponding Author

*Phone: +33 3 83 17 50 53. E-mail: raphael.schneider@ensic.inpl-nancy.fr.

■ ACKNOWLEDGMENT

This project is funded by the "EPST-Universités Lorraines". We also thank Dr. Ariane Boudier (EA 3452, Nancy-University) for FT-IR experiments.

■ REFERENCES

(1) Zheng, Y.; Gao, S.; Ying, J. Y. *Adv. Mater.* **2007**, *19*, 376.
(2) Moussodia, R. -O.; Balan, L.; Merlin, C.; Mustin, C.; Schneider, R. *J. Mater. Chem.* **2010**, *20*, 1147.
(3) Costa-Fernandez, J. M.; Pereiro, R.; Sanz-Medel, A. *Trends Anal. Chem.* **2006**, *25*, 207.
(4) Lim, J.; Jun, S.; Jane, E.; Baik, H.; Kim, H.; Cho, J. *Adv. Mater.* **2007**, *19*, 1927.
(5) Robel, I.; Subtamanian, V.; Kuno, M.; Kamat, P. V. *J. Am. Chem. Soc.* **2006**, *128*, 2385.
(6) Jamieson, T.; Bakhshi, R.; Petrova, D.; Pocock, R.; Imani, M. *Biomaterials* **2007**, *28*, 4717.
(7) Romero, M. J.; van de Lagemaat, J.; Mora-Sero, I.; Rumbles, G.; Al-Jassim, M. M. *Nano Lett.* **2006**, *6*, 2833.
(8) Yong, K. -T.; Roy, I.; Pudavar, H. E.; Bergey, E. J.; Tramposch, K. M.; Swihart, M. T.; Prasad, P. N. *Adv. Mater.* **2008**, *20*, 1412.
(9) Aldeek, F.; Balan, L.; Medjahdi, G.; Roques-Carmes, T.; Malval, J. -P.; Mustin, C.; Ghanbaja, J.; Schneider, R. *J. Phys. Chem. C* **2009**, *113*, 19458.
(10) Dabboussi, B. O.; Rodriguez-Viegro, J.; Mikulec, F. V.; Heine, J. R.; Mattoussi, H.; Ober, R.; Jensen, K. J.; Bawendi, M. G. *J. Phys. Chem. B* **1997**, *101*, 9463.
(11) Law, W. -C.; Yong, K. -T.; Roy, I.; Ding, H.; Hu, R.; Zhao, W.; Prasad, P. N. *Small* **2009**, *5*, 1302.
(12) Bhargava, R. N. *J. Lumin.* **1996**, *70*, 85.
(13) Norris, D. J.; Efros, A. L.; Erwin, S. C. *Science* **2008**, *319*, 1776.
(14) Hu, H.; Zhang, W. *Opt. Mater.* **2006**, *28*, 536.
(15) Beaulac, R.; Archer, P. I.; Gamelin, D. R. *J. Solid State Chem.* **2008**, *181*, 1582.

(16) Suyver, J. F.; Wuister, S. F.; Kelly, J. J.; Meijerink, A. *Phys. Chem. Chem. Phys.* **2000**, *2*, 5445.
(17) Kennedy, T. A.; Glaser, E. R.; Klein, P. B.; Bhargava, R. N. *Phys. Rev. B* **1995**, *52*, R14356.
(18) Meron, T.; Markovich, G. *J. Phys. Chem. B* **2005**, *109*, 20232.
(19) Pradan, N.; Goorskey, D.; Thessing, J.; Peng, X. *J. Am. Chem. Soc.* **2005**, *127*, 17586.
(20) Zu, L.; Norris, D. J.; Kennedy, T. A.; Erwin, S. C.; Efros, A. L. *Nano Lett.* **2006**, *6*, 334.
(21) Pradhan, N.; Battaglia, D. M.; Liu, Y.; Peng, X. *Nano Lett.* **2007**, *7*, 312.
(22) Pradhan, N.; Peng, X. *J. Am. Chem. Soc.* **2007**, *129*, 3339.
(23) Thakar, R.; Chen, Y.; Snee, P. T. *Nano Lett.* **2007**, *7*, 3429.
(24) Shen, H.; Wang, H.; Li, X.; Niu, J. Z.; Wang, H.; Chen, X.; Li, L. S. *Dalton Trans* **2009**, 10534.
(25) Zeng, R.; Rutherford, M.; Xie, R.; Zou, B.; Peng, X. *Chem. Mater.* **2010**, *22*, 2107.
(26) Acharya, S.; Sarma, D. D.; Jana, N. R.; Pradhan, N. *J. Phys. Chem. Lett.* **2010**, *1*, 485.
(27) Wang, C.; Gao, X.; Ma, Q.; Su, X. *J. Mater. Chem.* **2009**, *19*, 7016.
(28) Shao, P.; Zhang, Q.; Li, Y.; Wang, H. *J. Mater. Chem.* **2011**, *21*, 151.
(29) Fang, Z.; Wu, P.; Zhong, X.; Yang, Y.-J. *Nanotechnology* **2010**, *21*, 305604.
(30) Aboulaich, A.; Geszke, M.; Balan, L.; Ghanbaja, J.; Medjahdi, G.; Schneider, R. *Inorg. Chem.* **2010**, *49*, 10940.
(31) Kumbhojkar, N.; Nikesh, V. V.; Kshirsagar, A.; Mahamuni, S. *J. Appl. Phys.* **2000**, *88*, 6260.
(32) Chen, Y.; Rosenzweig, Z. *Anal. Chem.* **2002**, *74*, 5132.
(33) Rogach, A. L.; Kornowski, A.; Gao, M.; Eychmüller, A.; Weller, H. *J. Phys. Chem. B* **1999**, *103*, 3065.
(34) Kim, D. I.; Islam, M. A.; Avila, L.; Herman, I. P. *J. Phys. Chem. B* **2003**, *107*, 6318.
(35) Rogach, A. L.; Nagesha, D.; Ostrander, J. W.; Giersig, M.; Kotov, N. A. *Chem. Mater.* **2000**, *12*, 2676.
(36) Gaponik, N.; Talapin, D. V.; Rogach, A. L.; Hoppe, K.; Shevchenko, E. V.; Kornowski, A.; Eychmüller, A.; Weller, H. *J. Phys. Chem. B* **2002**, *106*, 7177.
(37) Zhang, H.; Wang, D.; Yang, B.; Möhwald, H. *J. Am. Chem. Soc.* **2006**, *128*, 10171.
(38) Privman, V.; Goia, D. V.; Park, J.; Matijevi, E. *J. Colloid Interface Sci.* **1999**, *213*, 6.
(39) Murray, C. B.; Kagan, C. R.; Bawendi, M. G. *Annu. Rev. Mater. Sci.* **2000**, *30*, 545.
(40) Shavel, A.; Gaponik, N.; Eychmüller, A. *J. Phys. Chem. B* **2004**, *108*, 5905.
(41) Wang, C.; Zhang, H.; Zhang, J.; Li, M.; Sun, H.; Yang, B. *J. Phys. Chem. C* **2007**, *111*, 2465.
(42) Klayman, D. L.; Griffin, T. S. *J. Am. Chem. Soc.* **1973**, *95*, 197.
(43) Cheery, R. W.; Coelho, A. A.; Cline, J. P. *J. Res. Natl. Stand. Technol.* **2004**, *109*, 1.
(44) Grabolle, M.; Spiles, M.; Lesnyak, V.; Gaponik, N.; Eychmüller, A.; Resch-Genger, U. *Anal. Chem.* **2009**, *81*, 6285–6294.
(45) Corbisier, P.; van der Lelie, D.; Borremans, B.; Provoost, A.; de Lorenzo, V.; Brown, N. L.; Lloyd, J. R.; Hobman, J. L.; Csoregi, E.; Johansson, G.; Mattiason, B. *Anal. Chim. Acta* **1999**, *387*, 235.
(46) Biebl, H.; Pfennig, N. *The Prokaryotes, a Handbook on Habitats, Isolation and Identification of Bacteria*; Springer-Verlag: Berlin, 1981; Vol. 1, pp 267−273.
(47) Blattner, F. R.; Plunkett, G., III; Bloch, C. A.; Perna, N. T.; Burland, V.; Riley, M.; Collado-Vides, J.; Glasner, J. D.; Rode, C. K.; Mayhew, G. F.; Gregor, J.; Davis, N. W.; Kirkpatrick, H. A.; Goeden, M. A.; Rose, D. J.; Mau, B.; Shao, Y. *Science* **1997**, *277*, 1453.
(48) Schneider, R.; Wolpert, C.; Guilloteau, H.; Balan, L.; Lambert, J.; Merlin, C. *Nanotechnology* **2009**, *20*, 225101.
(49) Ge, J. P.; Xu, S.; Zhuang, J.; Wang, X.; Peng, Q.; Li, Y. D. *Inorg. Chem.* **2006**, *128*, 4922.
(50) Qu, L. H.; Peng, X. G. *J. Am. Chem. Soc.* **2002**, *124*, 2049.
(51) Califano, M.; Franceschetti, A.; Zunger, A. *Nano Lett.* **2005**, *5*, 2360.
(52) Hines, M. A.; Guyot-Sionnest, P. *J. Phys. Chem.* **1996**, *100*, 468.
(53) Reiss, P.; Protière, M.; Li, L. *Small* **2009**, *5*, 154.
(54) Trintade, T.; O'Brian, P.; Pickert, N. L. *Chem. Mater.* **2001**, *13*, 3843.
(55) Jiang, D.; Cao, L.; Liu, W.; Su, G.; Qu, H.; Sun, Y.; Dong, B. *Nanoscale Res. Lett.* **2009**, *4*, 78.
(56) Bol, A. A.; Meijerink, A. *Phys. Rev. B* **1998**, *58*, R15997.
(57) Stewart, M. H.; Susumu, K.; Mei, B. C.; Medintz, I. L.; Delehanty, J. B.; Blanco-Canosa, J. B.; Dawson, P. E.; Mattoussi, H. *J. Am. Chem. Soc.* **2010**, *132*, 9804.
(58) Zheng, J.; Yuan, X.; Ikezawa, M.; Jing, P.; Liu, X.; Zheng, Z.; Kong, X.; Zhao, J.; Masumoto, Y. *J. Phys. Chem. C* **2009**, *113*, 16969.
(59) Liu, Y. S.; Sun, Y. H.; Vernier, P.; Liang, C. H.; Chong, S. Y. C.; Gundersen, M. A. *J. Phys. Chem. C* **2007**, *111*, 2872.